ELSEVIER

Polymer 40 (1999) 1917–1922

polymer

Birefringence in strong flows of polymer solutions

John M. Wiest*

Department of Chemical Engineering, University of Alabama, Tuscaloosa, AL 35487-0203, USA

Received 8 April 1998; revised 18 May 1998; accepted 28 May 1998

Abstract

The constitutive relation for the refractive index of dilute solutions of flexible polymer molecules is obtained, and calculations of the intrinsic birefringence exhibited in uniaxial elongational flow are presented. The polymer molecules are modeled as chains of beads connected by finitely extensible nonlinear elastic springs under the Peterlin approximation. It is found that at very low elongation rates there is very little birefringence, but there is a critical elongation rate above which there is substantial birefringence. This critical elongation rate scales as the inverse square of the number of beads in the chain. At this elongation rate the individual springs in the chains are stretched and oriented with the flow, but the chains have not uncoiled. It is found that the stress-optic relation holds for elongation rates below the critical elongation rate. However, the stress-optic coefficient is not constant above the critical rate. In the instantaneous inception of the flow above the critical elongation rate, the stress optic coefficient initially takes on the value that it would have below the critical elongation rate, but it decays to a much lower value as the strain increases.

Keywords: Birefringence; Stress-optic coefficient; Eigenvalue

1. Introduction

Dilute polymer solutions exhibit their most remarkable properties in strong flows. A flow is defined as being strong if the velocity gradient tensor has any eigenvalues with positive real part [1]. The most common examples of strong flows are shear-free flows in which the fluid is forced to move in such a manner that the velocity field in it is given by:

$$v_x = (-1/2)(1+m)\dot{\epsilon}x; v_y = (-1/2)(1+m)\dot{\epsilon}y; v_z = \dot{\epsilon}z. \quad (1)$$

Here $\dot{\epsilon}$ is the elongation rate, m is a parameter that describes the nature of the flow, and x, y and z are the spatial coordinates. Three special cases are usually considered: when $m = 0$ and $\dot{\epsilon} > 0$ the flow is called uniaxial elongational flow, when $m = 0$ and $\dot{\epsilon} < 0$ the flow is called biaxial stretching flow, and when $m = 1$ the flow is called planar elongational flow.

Dilute polymer solutions show unusual behavior in strong flows because these flows are capable of deforming the molecules substantially away from their equilibrium conformations. That is, the condition that the velocity gradient have eigenvalue(s) with positive real part(s) is sufficient for neighboring fluid elements to move away from one another exponentially fast, and this can cause appreciable stretching of the polymer molecules. This molecular stretching is thought to be a significant factor in phenomena such as drag reduction in turbulent flow and enhancement of jet stability. Consequently, the rheology of dilute polymer solutions in strong flows has been the subject of much study.

Because of the low viscosity of dilute polymer solutions, forcing them to undergo strong flows is a difficult task. Nonetheless, a number of ingenious ways to approximate strong flows have been devised. These include crossed slots [2–7] and four-roll mills [8–10] that approximate planar elongation in the region around the stagnation point in the flows. Another type of device that has been used to approximate strong flows employs converging channels [11–14], but the flow field in this type of geometry appears to be less homogeneous than those in the others. A frequently used device employs opposing nozzles or jets [15–23] that can approximate both uniaxial elongational flow and biaxial stretching flow. Most of these devices have been used to examine the optical properties of flowing polymer solutions. In particular, most have been used to examine the birefringence exhibited by the solutions at the stagnation point where the strong flow is approximated. Use of these devices to study the rheological properties of the fluids requires that some connection be made between the rheological properties and the birefringence. Only a few of the studies cited

* Tel: 001 205 348 6450.

0032-3861/99/$ - see front matter
PII: S0032-3861(98)00427-3

above have examined both optical and rheological properties [20–22].

Interest in uniaxial elongational flows of dilute polymer solutions has been re-ignited quite recently because of the development by Sridhar and co-workers [24–26] and by Spiegelberg and McKinley [27,28] of filament stretching devices. Such devices are exciting because they not only allow direct measurement of rheological properties, but can also provide simultaneous information about the optical properties (e.g. birefringence) of the liquids. In fact, recent measurements may indicate deviations from the stress-optic relation (G.H. McKinley, pers. comm.).

Recent theoretical studies of the behavior of dilute polymer solutions in strong flows have been concerned with the existence of coil-stretch transitions (see Refs. [29,30] and the papers cited therein). In addition, the behavior of polymer molecules in strong flows has been simulated by Acierno et al. [31], Rallison and Hinch [32], and Kobe and Wiest [33]. However, only the last of these studies has examined the birefringence shown by the system. Such an examination is the purpose of the modeling and calculations presented in this paper. We ask how the birefringence varies with elongation rate in steady uniaxial elongational flow and whether the stress-optic relation [34] is valid for these systems and these flows. We also consider the inception of uniaxial elongational flow in an attempt to more closely examine the experimental studies described above.

1.1. Refractive index of a polymer solution

We begin by describing the model that we use to describe a macromolecule in an infinitely dilute polymer solution. For brevity, we will use the notation of Bird et al. [35]. This model consists of a chain of N point masses ('beads') connected by $N-1$ massless springs. The chain configuration is described by a set of connector vectors $Q^{N-1}(=Q_1, Q_2, \ldots, Q_{N-1})$, where Q_i is the vector from the center of bead i to the center of bead $i+1$. The chain is described by a distribution of internal configurations, $\psi(Q^{N-1}, t)$, that is defined such that $\psi \mathrm{d}Q^{N-1}$ (where $\mathrm{d}Q^{N-1}$ denotes $\mathrm{d}Q_1\mathrm{d}Q_2\ldots\mathrm{d}Q_{N-1}$) is the probability that spring 1 is within $\mathrm{d}Q_1$ of Q_1, spring 2 is within $\mathrm{d}Q_2$ Of Q_2, and so on, at time t. We indicate integral averages over this distribution function by angular brackets. The distribution function is governed by a diffusion equation (cf. eqn 15.1–7) of Bird et al. [35]:

$$\frac{\partial\psi}{\partial t} = -\sum_j \frac{\partial}{\partial \mathbf{Q}_j}\cdot\left\{[\boldsymbol{\kappa}\cdot\mathbf{Q}_j]\psi - \frac{1}{\zeta}\sum_k A_{jk}\left[\mathrm{kT}\frac{\partial\psi}{\partial\mathbf{Q}_k} + Hf_k\mathbf{Q}_k\psi\right]\right\}. \tag{2}$$

In this equation, κ is the transpose of the macroscopic velocity gradient, ζ is the Stokes' law friction coefficient for an individual bead, A_{jk} is the Rouse matrix (consisting of twos along the diagonal, ones in the immediate off-diagonal elements, and zeros elsewhere) , kT is Boltzmann's constant times the absolute temperature, and H is a spring constant. The sums in Eq. (2) are over all of the springs in the chain (i.e. from 1 to $N-1$). It should be noted that this model does not incorporate any hydrodynamic or excluded volume interactions between beads. The f_k in Eq. (2) describe the tension in the springs; they are functions of the $\mathbf{Q}_k$,

It is possible to obtain an expression for the refractive index tensor for the polymer solution by considering each spring in the bead-spring chain to be composed of n_s links of a Kramers chain (i.e. a freely-jointed bead-rod chain). Each link of the Kramers chain is of length a and has parallel and perpendicular polarizability $\alpha_\parallel$ and $\alpha_\perp$, respectively. Then it can be shown [36] that the polarization tensor for a spring (spring i) is given by:

$$\alpha_i = \frac{n_s}{3}(\alpha_\parallel + 2\alpha_\perp)\delta + n_s(\alpha_\parallel - \alpha_\perp)\left[1 - \frac{3Q_i/n_s a}{L^{-1}(Q_i/n_s a)}\right]\frac{1}{Q_i^2}\left[\mathbf{Q}_i\mathbf{Q}_i - \frac{1}{3}Q_i^2\boldsymbol{\delta}\right], \tag{3}$$

where L^{-1} is the inverse Langevin function. In Eq. (3) we can recognize $n_s a$ as Q_0, the maximum length of the spring. The refractive index tensor, n, for the dilute solution taking into account the intrinsic birefringence is given by [37]:

$$\mathbf{n} = n\boldsymbol{\delta} + \frac{2\pi}{9n}(n^2+2)^2 c\tilde{N}\sum_i\left\langle \boldsymbol{\alpha}_i - \frac{1}{3}tr\alpha_i\boldsymbol{\delta}\right\rangle, \tag{4}$$

where n is the isotropic refractive index, c is the molar concentration of chains, and $\tilde{N}$ is Avogodro's number. Combining Eqs. (3) and (4), we have:

$$n = n\boldsymbol{\delta} + A\sum_i\left\langle \frac{1}{Q_i^2}\left(1 - \frac{3Q_i/Q_0}{L^{-1}(Q_i/Q_0)}\right)\left[\mathbf{Q}_i\mathbf{Q}_i - \frac{1}{3}Q_i^2\boldsymbol{\delta}\right]\right\rangle, \tag{5}$$

where we have defined a constant A by:

$$A = \frac{2\pi}{9n}(n^2+2)^2 c\tilde{N}n_s(\alpha_\parallel - \alpha_\perp). \tag{6}$$

This parameter is determined by the chemical structure of the macromolecule. Eq. (5) gives the refractive index tensor in terms of averages over the distribution of internal configurations. We can now, in principle, solve Eq. (2) for the distribution of internal configurations and use the result to evaluate the averages in Eq. (5).

However, we now introduce Warner's approximation [38,39] for the inverse Langevin function by the substitution:

$$L^{-1}(Q_i/Q_0) \rightarrow \frac{3Q_i/Q_0}{1-(Q_i/Q_0)^2}. \tag{7}$$

The resulting expression for the refractive index tensor is:

$$\mathbf{n} = n\boldsymbol{\delta} + \frac{A}{Q_0^2}\sum_i\left[\langle\mathbf{Q}_i\mathbf{Q}_i\rangle - \frac{1}{3}\langle Q_i^2\rangle\boldsymbol{\delta}\right]. \tag{8}$$

If we simplify the expression to a dumbbell (two beads, one spring), then we recover the result of Fuller [40].

We now introduce finitely extensible nonlinear elastic springs (FENE springs) [38,39]. For these springs the f_k are given by:

$$f_k = \left[1 - (Q_k/Q_0)^2\right]^{-1}, \tag{9}$$

where Q_0 is a parameter—the maximum extension of a spring. Eq. (9) arises as a result of an approximation suggested by Warner [38] for the inverse Langevin function. It is convenient to express results in terms of a dimensionless parameter $b = HQ_0^2/kT$. In the limit of infinite b we recover Rouse chains with Hookean springs.

We now introduce the Peterlin approximation [39,41,42] by rewriting Eq. (9) as:

$$f_k = \left[1 - (\langle Q_k^2\rangle/Q_0^2)\right]^{-1}. \tag{10}$$

That is, we replace the instantaneous extension of the spring in Eq. (9) by the root-mean-square extension at the prevailing kinematic condition. With this approximation, the set of moment equations generated from the diffusion equation is closed at those equations for the second moments. These equations are obtained by multiplying Eq. (2) by the dyad $\mathbf{Q}_i\mathbf{Q}_j$ and integrating the resulting equations over all $\mathbf{Q}^{N-1}$. The results are:

$$\frac{d}{dt}\langle \mathbf{Q}_i\mathbf{Q}_j\rangle = \boldsymbol{\kappa}\cdot\langle \mathbf{Q}_i\mathbf{Q}_j\rangle + \langle \mathbf{Q}_i\mathbf{Q}_j\rangle\cdot\boldsymbol{\kappa}^{\dagger} + (2\mathrm{kT}/\zeta)A_{ij}\boldsymbol{\delta} - (H/\zeta)\sum_k f_k\left[A_{ik}\langle \mathbf{Q}_k\mathbf{Q}_j\rangle + A_{jk}\langle \mathbf{Q}_i\mathbf{Q}_k\rangle\right], \tag{11}$$

where the f_k are given by Eq. (10), and δ is the second-order unit tensor. The superscript dagger indicates the transpose of a tensor. The initial conditions for Eq. (11) are provided by the equilibrium distribution function corresponding to the spring forces given by Eq. (10). They are:

$$\langle Q_iQ_j\rangle \to \frac{Q_0^2}{b+3}\delta_{ij}\delta \text{ as } t \to -\infty, \tag{12}$$

where δ_{ij}, is the Kronecker delta. All of the quantities that we calculate here can be expressed in terms of the second moments of ψ. In fact, under the Peterlin approximation the set of second moments completely describes the distribution of configurations. That is, the chain is Gaussian but with time and kinematic dependent covariances that are determined by the restriction that the root mean square extensions of the springs not exceed Q_0.

It is significant to note that the form of Eq. (8) does not rely on the Peterlin approximation. That is, if we were to apply the Peterlin approximation in Eq. (5), we would obtain the same results. Of course, the Peterlin approximation does have an effect on the values taken on by the second moment tensors appearing in Eq. (8).

In order to test the validity of the stress-optic relation for this system, we also calculate the stresses predicted by the model. The expression for the polymer contribution to the stress tensor is (36):

$$\boldsymbol{\tau}_p = (N-1)n_p\mathrm{kT}\boldsymbol{\delta} - n_pH\sum_k f_k\langle \mathbf{Q}_k\mathbf{Q}_k\rangle. \tag{13}$$

In this expression, n_p is the number density of chains. The first term on the right-hand side of Eq. (13) arises as a result of the inertia of the beads. The remaining terms are the contributions to the stress from the tensions in the springs. The f_k are given by Eq. (10).

1.2. Steady uniaxial elongational flow

In uniaxial elongational flow, Eq. (8) predicts that the intrinsic birefringence is given by:

$$\Delta n = n_{zz} - n_{xx} = \frac{A}{Q_0^2}\sum_i\left[\langle Q_{iz}Q_{iz}\rangle - \langle Q_{ix}Q_{ix}\rangle\right]. \tag{14}$$

In Eq. (14), Q_{ik} is the kth component of the vector $\mathbf{Q}_i$. To determine the moment components in Eq. (14), we solve Eqs. (11) and (12) as a set of coupled nonlinear ordinary differential equations (in time) for the second moments with a fourth-order Runge–Kutta routine. Steady flow predictions are determined as the long time asymptotes of the transient solutions.

In Fig. 1 we present the birefringence predicted by the model in steady uniaxial elongational flow (i.e. constant $\dot{\epsilon}$) for chains of varying numbers of beads. The elongation rate is made dimensionless by multiplying it by a time constant defined by $\lambda_H = \zeta/4H$. At low elongation rates, the birefringence is very small. Then at a critical elongation rate the birefringence increases dramatically. This is in agreement with the observations of Keller et al. [2,4–6]. The critical elongation rate scales as the inverse square of the number of beads in the chain. Keller et al. [2,4–6] observed experimentally that the critical elongation rate in their experiments scaled as approximately the inverse 1.5 power of the molecular weight. This difference is probably a consequence of hydrodynamic interactions. The birefringence saturates

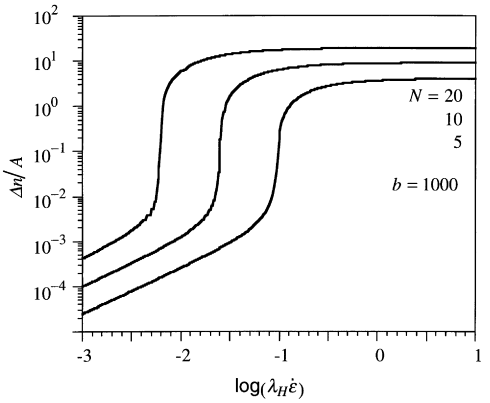

Fig. 1. The birefringence predicted for chains of varying number of beads in steady uniaxialelongational flow. There is a critical elongation rate below which the birefringence is very small. This critical elongation rate scales as N^{-2}.

(approaches its large elongation rate asymptote) at relatively small values of the dimensionless elongation rate.

The intrinsic birefringence is independent of the parameter b indicating that it depends upon only the fractional extensions of the springs and not their total extensions. However, we should expect that the total birefringence would depend on the length of the springs because of contributions from form birefringence. The predictions shown in Fig. 1 are qualitatively very similar to the measurements of Cathey and Fuller [22].

The stress-optic relation predicts that the stress tensor should be proportional to the index of refraction tensor [34]. The relation was originally derived from a Gaussian network model for crosslinked rubber [43]. For uniaxial elongational flow, the relation states that:

$$\frac{\Delta n}{\tau_{p,xx} - \tau_{p,zz}} = C, \tag{15}$$

where C is a constant (independent of the elongation rate) called the stress-optic coefficient. Our predictions for this ratio (in dimensionless form) are given in Fig. 2 for chains of varying numbers of beads. At very low elongation rates the relation does hold. However, above the critical elongation rate where the birefringence increases in Fig. 1, the relation no longer holds. At these larger elongation rates the 'constant' decays almost linearly with the reciprocal of the elongation rate.

We can interpret these results in terms of the conformation and properties of the chains. In Fig. 3 we present the mean square end-to-end distance for the chains and the average moment of inertia about the principal flow axis (the z-axis). The latter is given in terms of the second moments of the distribution of internal configurations by:

$$\frac{\langle I_{zz}\rangle}{\langle I_{zz}\rangle_{eq}} = \frac{3(b+3)}{(N^2-1)Q_0^2}\sum_{ij} C_{ij}\langle Q_{ix}Q_{jx} + Q_{iy}Q_{jy}\rangle, \tag{16}$$

where C_{ij} is the Kramers matrix (the inverse of the Rouse matrix). That is, I_{zz} is the zz component of the moment of inertia tensor for a chain defined by: $I = \sum_\nu m_\nu\{(R_\nu \cdot R_\nu)\delta - R_\nu R_\nu\}$, where m_ν is the mass of a bead, R_ν the position of the νth bead relative to the center-of-mass of the chain, and the sum extends over all of the beads in a chain. The zz component of the average moment of inertia tensor is a good measure of conformations because it is equal to zero when the chains are, on average, completely aligned in the flow direction.

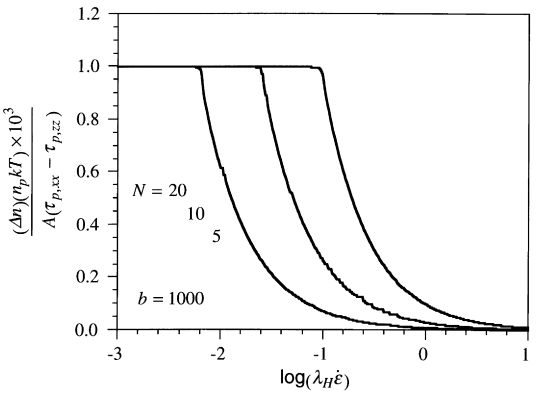

Fig. 2. A test of the stress-optic relation in steady uniaxial elongational flow for chains of varying numbers of beads. The relation holds at low elongation rates, but above the critical elongation rate observed in Fig. 1, the relation no longer holds.

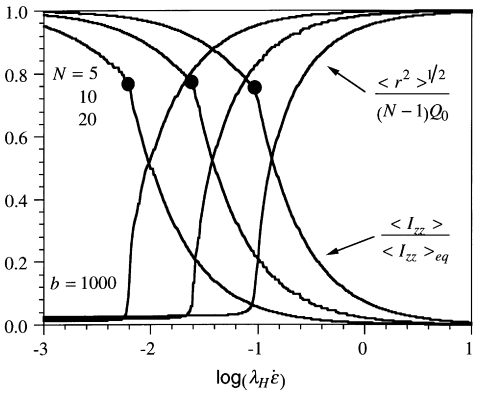

Fig. 3. The mean square end-to-end distance and average moment of inertia about the principal flow axis for chains of varying numbers of beads in steady uniaxial elongational flow The solid points indicate the critical elongation rates that were observed in Fig. 1.

The solid points in Fig. 3 indicate the critical elongation rate at which the birefringence increases significantly. We see that the birefringence increases dramatically when the moment of inertia is less than about 75% of its equilibrium value. The points also correspond to the elongation rates at which the mean square end-to-end distance begins to increase significantly in Fig. 3. At the critical elongation rates, the decrease in the moment of inertia indicates that the individual springs are stretched and oriented with the flow [30], but the small value for the mean square end-to-end distance indicates that the entire chain has not become uncoiled. We see that alignment of individual springs with the flow gives the most significant contribution to the intrinsic birefringence.

1.3. Inception of uniaxial elongational flow

We now turn our attention to the inception of uniaxial elongational flow where $\dot{\epsilon}(t) = \dot{\epsilon}_0 H(t)$ with $H(t)$ being the Heaviside unit step function. This is the flow that is examined in filament stretching devices [24–28], and it also more closely approximates the flow obtained in opposing nozzle devices [15–23] in that individual molecules experience a transient elongation as they approach the stagnation point in the apparatus. At very low elongation rates, the stress-optic coefficient is constant. That is, at low elongation rates the stresses and birefringence grow to their steady state values with the same time dependence. This growth is indicated in Fig. 4 where Δn_{ss} is the steady flow value of the birefringence. In that figure we also show the average moment of inertia of the chains about the principal flow axis. This indicates that the birefringence reaches its steady-flow

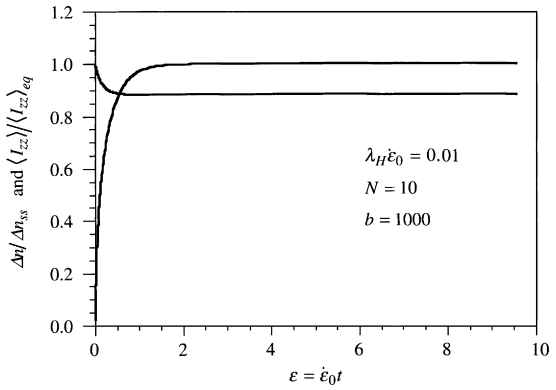

Fig. 4. The growth of the birefringence and the decay of the moment of inertia about the principal flow axis for the inception of uniaxial elongational flow at an elongation rate that is below the critical elongation rate. At this elongation rate the stress-optic coefficient is constant (i.e. independent of time).

value as the chains reach their average steady-flow conformations which are primarily coiled [30].

In Fig. 5 we show these quantities for the inception of flow at an elongation rate that is greater than the critical elongation rate. At this elongation rate we observe that the initially spherical envelope enclosing the molecules becomes substantially aligned by the flow ($\langle I_{zz}\rangle$ decreases markedly with time). This alignment is paralleled by a substantial increase in the birefringence. The 'knee' that occurs in the $\langle I_{zz}\rangle$ curve at a Hencky strain of about four is interpreted by Wiest et al., [30] as being the point at which the individual springs in the chain stretch to near their maximum extensions (before the chain unfolds and becomes linear). This is the strain at which the birefringence shows its marked increase. Actual unfolding of the chain does not effect the intrinsic birefringence (although it would effect the total birefringence through form birefringence).

Fig. 6 shows the stress-optic coefficient as a function of time from the inception of uniaxial elongational flow at several elongation rates. As mentioned above, at the lowest elongation rate (which is below the critical elongation rate) the stress optic coefficient is constant. At higher elongation

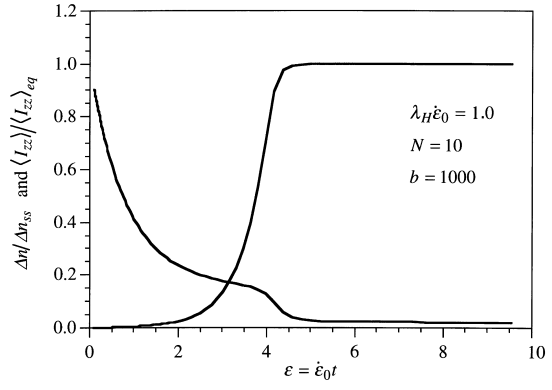

Fig. 5. The growth of the birefringence and the decay of the moment of inertia about the principal flow axis for the inception of uniaxial elongational flow at an elongation rate that is above the critical elongation rate.

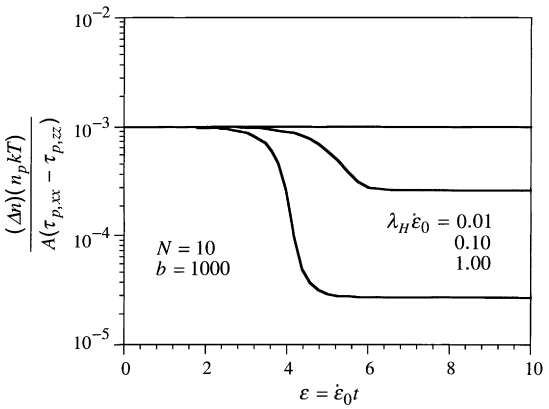

Fig. 6. The stress-optic coefficient as a function of strain in the inception of uniaxial elongational flow at several elongation rates The two higher elongation rates are above the critical rate. Note that there is a substantial period of time (strain) after the inception of the flow during which the coefficient is nearly constant.

rates (above the critical elongation rate) the birefringence responds to the inception of flow before the stresses, and the coefficient is not constant. However, there is a considerable period of time (strain) after the inception of the flow during which the coefficient is nearly constant. Furthermore, this 'constant' is the same value that the coefficient would take at elongation rates below the critical rate.

2. Summary

In summary we can conclude that in steady uniaxial elongational flow there is a critical elongation rate below which there is very little intrinsic birefringence and above which the birefringence increases substantially. For the particular model that we considered, the critical elongation rate scales as the inverse square of the elongation rate. Furthermore, the stress-optic relation is valid below this critical elongation rate, but it does not hold for larger rates. This is disappointing because it indicates that it may not be possible to use optical techniques to measure stresses in steady strong flows of dilute polymer solutions.

Our results for non-steady flow indicate that the stress-optic coefficient is a function of time as well as elongation rate. However, the transient results indicate that, above the critical elongation rate, the stress-optic coefficient retains the value that it would have below the critical elongation rate for a considerable period of time (strain).

In spite of the perhaps disappointing consequences of the results presented here regarding the use of birefringence measurements as a probe of the elongational rheological properties of dilute polymer solutions, the results may prove to be quite useful in the study of the process whereby molecules uncoil in strong flows. Differences in rheological property predictions of various molecularly-based theories seem to be somewhat insensitive for examination of this process, and birefringence measurements may be much more useful.

Acknowledgements

The author gratefully acknowledges the financial support of the Donors of the Petroleum Research Fund and E.I. du Pont de Nemours and Co. He also wishes to thank Professors R.B. Bird, D.F. James, and Roland Keunings for helpful discussions.

References

[1] Tanner RI, Huilgol RR. Rheol Acta 1975;14:959–962.
[2] Miles MJ, Keller A. Polymer 1980;21:1295–1298.
[3] Lyazid A, Scrivener O, Teitgen R. In: Astarita G, Marrucci P, Nicolais L, editors. Rheology, vol. 2. New York: Plenum Press, 1980:141–148.
[4] Gardener K, Pike EP, Miles MJ, Keller A, Tanaka K. Polymer 1982;23:1435–1442.
[5] Odell JA, Keller A, Miles MJ. Polymer 1985;26:1219–1226.
[6] Odell JA, Keller A. J Polym Sci, Polym Phys Ed 1986;24:1889–1916.
[7] Farinato RS. Polymer 1988;29:160–167.
[8] Pope DP, Keller A. Colloid Polym Sci 1977;255:633–643.
[9] Fuller GG, Leal LG. Rheol Acta 1980;19:580–600.
[10] Dunlap PN, Leal LG. J Non-Newtonian Fluid Mech 1987;23:548.
[11] Chauveteau G, Moan M, Magueur A. J Non-Newtonian Fluid Mech 1984;16:315–327.
[12] James DF, McLean BD, Saringer JH. J Rheo l1987;31:453–481.
[13] Wunderlich AM, James DF. Rheol Acta 1987;26:522–531.
[14] Mackley MR, Keller A. Phil Trans, R Soc (Lond) 1975;278:29–66.
[15] Pope DP, Keller A. Colloid Polym Sci 1978;256:751–756.
[16] Farrell CJ, Keller A, Miles MJ, Pope DP. Polymer 1980;21:1292–1294.
[17] Peiffer DG, Kim MW, Lundberg RD. Polymer 1986;27:493–502.
[18] Peiffer DG, Kim MW, Schuiz DN. J Polym Sci, Polym Phys Ed 1987;25:1615–1628.
[19] Fuller GG, Cathey CA, Hubbard B, Zebrowski BE. J Rheol 1987;31:235–249.
[20] Chow A, Keller A, Muller AJ, Odell JA. Macromolecules 1988;21:250–256.
[21] Odell JA, Muller AJ, Keller A. Polymer 1988;29:1179–1190.
[22] Cathey CA, Fuller GG. J Non-Newtonian Fluid Mech 1990;34:63–88.
[23] Odell JA, Muller AJ, Narh KA, Keller A. Macromolecules 1990;23:3092–3103.
[24] Tirtaatmadja V, Sridhar T. J Rheol 1993;37:1081–1102.
[25] Tirtaatmadja V, Sridhar T. J Rheol 1995;39:1133–1160.
[26] Orr NV, Sridhar T. J Non-Newtonian Fluid Mech 1996;67:77103.
[27] Spiegelberg SH, McKinley GH. In: Ait-Kadi A, Dealy JM, James DF, Williams MC, editors. Proceedings of the 12th International Congress on Rheology. Laval University Press, 1996.
[28] Spiegelberg SH, McKinley GH. J Non-Newtonian Fluid Mech 1996;67:49–76.
[29] Wiest JM, Wedgewood LE, Bird RB. J Chem Phys 1989;90:587–594.
[30] Acierno D, Titomanlio G, Marrucci G. J Polym Sci, Polym Phys Ed 1974;12:2177–2187.
[31] Rallison JM, Hinch EJ. J Non-Newtonian Fluid Mech 1988;29:37–55.
[32] Kobe JM, Wiest JM. J Rheol 1993;37:947–960.
[33] Janeschitz-Kriegi H. Polymer melt rheology and flow birefringence. Berlin: Springer, 1983.
[34] Bird RB, Curtiss CF, Armstrong RC, Hassager O. Dynamics of polymeric liquids, vol. 2, kinetic theory, 2nd edn. New York: Wiley, 1987.
[35] Flory PJ. Statistical mechanics of chain molecules. New York: Wiley, 1969.
[36] Doi M, Edwards SF. The theory of polymer dynamics. Oxford: Oxford Science, 1986:219.
[37] Warner HR Jr. Ind Eng ChemFund 1972;11:379–381.
[38] Wiest JM, Tanner RI. J Rheol 1989;33:281–316.
[39] Fuller GG. Ann Rev Fluid Mech 1990;22:387–417.
[40] Peterlin A. J Polym Sci, Polym Lett Ed 1972;4:287.
[41] Peterlin A. Makromol Chem 1966;44:338.
[42] Treloar LRG. The physics of rubber elasticity, 2nd edn. Oxford: Oxford Press, 1958.
[43] Fan XA, Bird RB, Renardy MJ. J Non-Newtonian Fluid Mech 1985;18:255.